UNIVERSITY OF CALIFORNIA SAN DIEGO

Longitudinal Imaging of Cortical and Sub-cortical Inputs to Primary Motor Cortex During Motor Learning

A thesis submitted in partial satisfaction of the requirements for the degree Master of Science

in

Biology

by

Yuxin Hu

Committee in charge:

Professor Takaki Komiyama, Chair
Professor Matthew Banghart
Professor Jill Leutgeb

2021

The thesis of Yuxin Hu is approved, and it is acceptable in quality and form for publication on microfilm and electronically.

University of California San Diego

2021

TABLE OF CONTENTS

Thesis Approval Page..... iii

Table of Contents..... iv

List of Abbreviations..... v

List of Figures..... vi

Acknowledgments..... vii

Abstract of the Thesis..... viii

Introduction..... 1

Methods..... 4

Results..... 10

Discussion..... 23

References..... 25

LIST OF ABBREVIATIONS

cM1 – Contralateral Primary Motor Cortex

CT – Corticothalamic

IT – Intratelencephalic

M1 – Primary Motor Cortex

PT – Pyramidal Tract

ROI – Region of Interest

S1 – Primary Somatosensory Cortex

LIST OF FIGURES

Figure 1: Experimental scheme ……11

Figure 2: Histology slices of 3 projections in mScarlet ……12

Figure 3: Behavioral changes during the 14-day motor learning ……13

Figure 4: Binarized behavior traces aligned to axonal bouton activity ……14

Figure 5: Classification of axonal boutons across projection sites ……17

Figure 6: Individual deconvolved spikes of movement-related axonal boutons aligned to movement ……..19

Figure 7: Averaged deconvolved spikes of movement-related axonal boutons aligned to movement onset and offset ……20

Figure 8: Movement-related boutons grouped into 4 clusters based on peak time in the temporal sequence ……21

Figure 9: Pairwise comparison of individual axonal bouton activity across trials ……22

ACKNOWLEDGEMENTS

I would like to acknowledge Professor Takaki Komiyama for his support as the chair of my committee. His support and guidance helped me find the direction to make progress in this project.

I would like to acknowledge Assaf Ramot, who served as my project supervisor. As a mentor, Assaf taught me many techniques, established the experiment pipelines, and helped me with data analysis. It would be impossible to finish this project without him.

I would also like to acknowledge Dr. Ofer Yizhar from Weizmann Institute of Science. A large part of the experiment was done with using the eOPN3 plasmids he gifted to us. This project would be incomplete without eOPN3.

ABSTRACT OF THE THESIS

Longitudinal Imaging of Cortical and Sub-cortical Inputs to Primary Motor Cortex During Motor Learning

by

Yuxin Hu

Master of Science in Biology

University of California San Diego, 2021

Professor Takaki Komiyama, Chair

The primary motor cortex (M1) is critical for motor learning and performance, and it is heavily innervated by inputs from the contralateral M1 (cM1), the primary somatosensory cortex (S1), and the motor thalamus. M1 integrates these inputs and sends out divergent outputs to different brain regions. To decipher how this relay system functions, we investigated the major M1 inputs in order to find whether there is a unique activity pattern and functional role for each

input. Here, we used two-photon calcium imaging in order to record the Calcium traces of axons originating from cM1, S1 and motor thalamus, while mice were trained in a motor learning task. In addition, we selectively suppressed neurotransmitter release at synaptic terminals from each of the above projections, in order to investigate the effect of inhibiting of M1 inputs on behavior. We found these three types of inputs appear to be different from each other in terms of peak time and consistency of a single axonal bouton's activity pattern across trials. Therefore, we proposed the activity patterns for cM1, S1, and thalamocortical inputs innervating M1 are different, and the different functional roles of each brain region might account for the variabilities in activity patterns.

Introduction:

Motor learning refers to changes in the ability to execute a motor skill and is fundamental for the well-being of many animal species, including humans. Studies performed in rodents have shown that M1 is critical for certain motor skills, especially goal-directed movement (Chen et al., 2015). In the cued lever-press task, a motor learning paradigm developed by the Komiyama lab, and which was used in the current work, M1 is necessary for the learning and execution of the task during the first several weeks of training (Chen et al., 2015; Makino et al., 2017; Peters et al., 2014, 2017). Mice exhibit learned motor skills by repeatedly performing a goal-directed movement pattern throughout the early training sessions. Movements in an extended training period can be independent of M1 activity (Hwang et al., 2019). Regardless of training time, M1 is not required for all learned movements, as previously shown by M1 lesions which did not have clear effects on the execution of certain motor skills (Kawai et al., 2015). Although M1 has essential roles in motor learning and execution (Peters et al., 2017), its precise function, especially in rodents is still a topic of study. Therefore, we focused on the initial period of motor learning and execution to study the functions dependent on M1.

Different layers of M1 neurons have different communication patterns. The flow of information is top-down, from the surface to the deep layers (Weiler et al., 2008). Intratelencephalic (IT)-type neurons project to other cortical areas and the striatum from the upper layers (L2/3 and L5A). These neurons within L2/3 are the focus of this study since they exhibit high dynamism during the initial phase of learning and their activity is correlated with movement during motor learning (Peters et al., 2014). Moreover, during motor learning, the number of new dendritic spines on the apical dendrites of these L2/3 neurons increases. (Chen et al., 2015; Peters et al., 2014). This growth can be blocked by artificial inhibition from somatostatin-expression

inhibitory neurons. Inhibited spine plasticity and behavioral improvement confirmed the critical role of M1 L2/3 neurons in motor learning (Chen et al., 2015).

Despite the importance of the motor cortex in motor learning and performance, the motor cortex does not facilitate motor control and learning on its own, rather it is a part of a relay system, in which it receives convergent information, integrates diverse motor-related signals, and sends divergent outputs to many other brain areas (Hooks et al., 2013; Penhune and Steele, 2012). However, how this relay system works is still not well understood. Therefore, in order to gain a better understanding of M1's function in supporting motor learning and execution, our main research aim was to examine the activity patterns of principal inputs innervating M1 during motor learning.

M1 is heavily innervated by other cortical areas and the motor thalamus (Muñoz-Castañeda et al., 2020). Within the sub-cortical area, motor thalamus is the main source that projects to M1 (Muñoz-Castañeda et al., 2020). Studies have shown that the thalamocortical axons within M1 L2/3 are active the most during the initial and terminal phases of the execution of learned movements (Tanaka et al., 2018). These thalamocortical inputs, therefore, are critical for learned motor skills (Sauerbrei et al., 2020). Within the cortical areas, cM1, S1, and the premotor cortex are the three major regions that generate the largest inputs. Both cM1 and S1 project heavily to M1 (Hooks et al., 2013; Muñoz-Castañeda et al., 2020). cM1 projections can innervate neurons in all layers of M1(Muñoz-Castañeda et al., 2020). S1 inputs are involved in sensorimotor integration and were shown in electrophysiological studies that it is able to excite both M1 L2/3 and L5A neurons (Petrof et al., 2015). The transient stimulation can be immediately seen in postsynaptic M1 L2/3 cells (Petrof et al., 2015). However, in contrast, projections from premotor cortex are mainly observed to be innervating neurons within deep layers of M1 (Hira et al., 2013). Therefore,

the three major inputs we study here are cM1, S1, and motor thalamus, not including the premotor cortex.

Methods:

Animals

All procedures adhered to the protocols approved by the University of California, San Diego Institutional Animal Care and Use Committee as well as the National Institutes of Health guidelines. Male and female mice were acquired from Charles River Laboratory (C57Bl/6 wild-type mice) and The Jackson Laboratory (Vglut2-ires-cre mice). Group-housed animals were placed in disposable plastic cages with standard bedding and nestlets. Singly housed animals were provided with a running wheel. All animals were kept in a room with a reversed light cycle (12 h-12 h). All experiments and perturbations happened during nighttime at approximately the same time each day.

Surgery

Surgeries are performed as described in (Makino et al., 2017; Peters et al., 2014). For two-photon calcium imaging adult mice (male and female, between 6 weeks to 4 months old) were anesthetized with isoflurane. Before scalp was removed, betadine and ethanol were applied to prevent infections. After the skull was exposed, bregma was marked as a reference point for the marking of M1 and the injection site. Coordinates for the injection sites: cM1 AP 0.3 mm; ML -1.5 mm (left hemisphere), DV -0.5/-0.25 mm; S1 AP -0.5 mm; ML 2.5 mm (right hemisphere), DV -0.5/-0.25 mm; Thalamus AP -1.0 mm; ML 1.0 mm (right hemisphere), DV -3.7 mm. To inject viral vectors, C57Bl/6 wild-type mice were used for cM1 and S1 viral vector injections; Vglut2-ires-cre (Jax 016963) mice were used for thalamocortical injections. AAV1-CMV-PI-Cre-rBG (AddGene 105537) and AAV-hSyn-FLEX-axon-GCaMP6s (AddGene 112010) with 1:2 dilution was front-loaded into a glass pipette and injected into cM1 (±50 nL at -0.5 mm and ±50 nL at -0.25 mm from pia) and S1 (±20 nL at -0.5 mm and ±20 nL at -0.25 mm from pia); AAV-hSyn-

FLEX-axon-GCaMP6s (AddGene 112010) was injected into the thalamus (±100 nL at -3.7 mm from pia). For optogenetic inactivation of axons, pAAV-CKIIa(0.4)-eOPN3-mScarlet was injected into the cM1 (±75 nL at -0.5 mm and ±75 nL at -0.25 mm from pia) and S1 (±30 nL at -0.5 mm and ±30 nL at -0.25 mm from pia); pAAV-hSyn1-SIO-eOPN3-mScarlet was injected into the motor thalamus (±150 nL at -3.6 mm from pia). AAV-syn-jGCaMP7b-WPRE (AddGene 104489) was used in the two animals but given that axon-GCaMP6s has many advantages including being able to display bright axonal and bouton labeling, GCaMP7b was not continued to be used (Broussard et al., 2018). Each injection was done at a rate of 20 nL per minute. The glass pipette was left in the brain for 5-15 min to prevent backflow. After virus injections, the skull was scratched with a blade to create better adhesion. A custom head-plate was then fixed onto the skull with superglue followed by dental cement.

After the placing of a headplate, craniotomy was performed as described over the right M1 area (AP +0.3 mm; ML ±1.5 mm) (Holtmaat et al., 2009). A circular piece of scalp was removed. Underlying bones were removed by a pair of forceps. A chronic imaging window consisting of a glass plug glued onto a larger glass base was implanted (Komiyama et al., 2010). Buprenorphine (0.1 mg/kg body weight) and Baytril (10 mg/kg body weight) were injected subcutaneously at the end of surgery. One week after surgery, Dexamethasone (10 mg/kg body weight) and Baytril (10 mg/kg body weight) were given to prevent infections.

Behavior

Two weeks after mice were recovered from the surgery, they were water restricted to 1mL per day. After ~14 days of water restriction, mice were trained to perform a water reward lever-press task with simultaneous two-photon imaging. Imaging session takes place every day over 14 days. The behavior setup was controlled by software (Dispatcher, Z. Mainen and C. Brody)

running on MATLAB with a real-time system (RTLinux). In each trial, a mouse would first hear a 6 kHz auditory cue (up to 10 s) in each cue period. Then a successful lever press would be rewarded with ~10 μL water from the lick port followed by an inter-trial interval (8-12 sec). Licking of the lick port was detected by a touch detector (Slotnick, 2009). A successful lever press was defined as crossing of two thresholds (~1.5 mm and ~3 mm below the resting position) within 200 ms. The lever position was continuously monitored through a piezoelectric flexible force transducer using LabVIEW (National Instruments). Two thresholds can make sure the mouse is performing a successful lever press reaching a 3 mm displacement, and it is not holding the lever near the lower threshold. Failure to perform the task can lead a loud white noise as punishment followed by an inter-trial interval. Rewards and punishments happen only during the cue period. Each training session was 100 trials. Along with licking, the lever position was constantly recorded by Ephus in MATLAB (MathWorks). Mice that failed to learn the task were excluded from analyses.

Two-photon calcium imaging

Along with the lever-press task, imaging was conducted with a commercial two-photon microscope (Thorlabs), which is equipped with a resonant galvanometric system, a large-NA 16 x objective lens (Nikon), and excitation light at 925 nm from a Ti-Sa laser (Newport) controlled by ScanImage (Vidrio Technologies). Images were recorded at ~30 frames/sec, and recorded frames were aligned with behavioral data from Ephus and also processed using Suite2p software (Pachitariu et al., 2017). A 1x image containing blood vessels and axons at upper layer was recorded as a guide, which was used to locate the same field of view (FOV) across the 14 days of recording. To record L2/3 axons, FOV's were approximately 250 mm deep from dura. During

each session, a reference image was taken to manually correct slow drifts in the FOV. 7 mice were imaged for cM1 projection; as for S1 and motor thalamus, 5 mice were recorded for each.

Optogenetic Inactivation

pAAV-CKIIa(0.4)-eOPN3-mScarlet was injected into cM1 and S1 of C57Bl/6 wild-type mice; pAAV-hSyn1-SIO-eOPN3-mScarlet was injected into motor thalamus of Vglut2-ires-cre mice. eOPN3 can effectively suppress synaptic transmission through the $G_{i/o}$ pathway (Mahn et al., 2021). A brief pulse at the presynaptic terminals triggers suppression of synaptic output up to ~5 min and recovers after ~5 min (Mahn et al., 2021). Two weeks after the surgery, cranial windows were covered with curable silicone (KWIK-CAST, World Precision Instruments), and mice were water restricted to 1 mL per day. After 14 days of water restriction, same behavior paradigm was performed. After 7 sessions of training, curable silicone was removed, and internal controls were conducted during the following 7 sessions. 100 trials were divided into 5 internal blocks: trial 1-20 were control block; 21-40 were suppression block; 41-60 were recovery block; 61-80 were control block; and 81-100 were suppression block. Calcium events in M1 L2/3 were reduced following 3 seconds of 532 nm green illumination (532 nm laser, 30mW) (Mahn et al., 2021). Optogenetic inactivation was done on 3 animals following this protocol, one for each injection site. Optogenetic sessions started on day 11 for 4 animals, and 3 seconds of 660 nm red LED (90mW) without filter was applied for inactivation. Same set-up for the internal blocks was used.

Image Analysis

Suite2p software was used to process calcium signals and extract region of interest (ROIs). Calcium signals were processed into $\Delta F/F$ traces and deconvoluted spikes (Pachitariu et al., 2017).

Movement Analysis

During each session, the voltage from the piezoelectric lever was continuously recorded at 10 kHz and parsed into movement and quiescence epochs as previously described (Peters et al., 2014). The velocity threshold was used to detect movement first. After that, movement epochs were refined by combining nearby epochs, eliminating small epochs, and refining the start and end times of movement epochs based on when the lever position left or entered a baseline defined by adjacent quiescent epochs. Visual inspection confirmed that the behavior was accurately demarcated.

Movements used for analyses were not limited to only those that resulted in a reward in order to make the most of the data. Movements made during the intertrial interval or unsuccessful movements made during the response period were also analyzed in this case. Relationship between movements and activity was analyzed using 3 sec starting from one second before the onset of each movement, and 2 sec following movement onset.

Classification of Movement-related Axonal Boutons

Axonal boutons whose activity was significantly higher during movement periods were classified as movement related using as described in detail (Peters et al., 2014). Briefly, the amount of activity during movement was calculated for each ROI as the mean value of the activity event trace during movement epochs. The movement trace was then shuffled (1000 times) such that complete movement epochs were kept intact but their position in the trace and relation to each other was randomized. A measure of activity during these shuffled movement epochs was calculated in each shuffle as above. An ROI was classified as movement-related if the real value was higher than the 0.5 percentile value of the shuffled values.

Perfusion & Histology

After imaging and optogenetic sessions, animals were anesthetized and transcranially perfused with ice-cold 0.1M PBS (PH 7.4), followed by perfusion with 4% Paraformaldehyde (PFA) solution for brain extraction. After brains were extracted, they were stored in 4% PFA for 1-2 days at 4 °C before they were transferred to 30% sucrose solution. When the brains had sunk to the bottom of the solution, they were ready to be sliced. Brains were cut coronally into 60 μm slices using a microtome (Thermo Scientific Microm HM 430), collected in PBS, and mounted to microscope glass slides (Fisherbrand 12-550-15) with CC/mount (Sigma MKCM4302). Mounted slices were visualized with a Zeiss Imager M2 with the Apotome.2 attachment, controlled by AxioVision 4.8 software. Images of the injection and projection sites were captured under a Confocal microscope with Leica LAS X LS software.

Statistics

In order to compare the activity of each input, deconvolved spike traces were binned into pre-movement periods (1s before onset), movement-onset period (movement-onset to 1 sec post movement-onset), and post-onset period (1 sec post movement-onet to 2 seconds post movement-onset. Deconvolved spikes for each bin were compared across inputs using One-way ANOVA followed by 'Tukey-Kramer' multiple comparisons. Movement-off set traces were binned similarly.

Results:

In order to functionally image the primary inputs M1 receives, axonal GCaMP6s was used for viral labeling of three main input axons of M1, two cortical areas - contralateral M1 (cM1) and primary somatosensory cortex (S1), as well as the motor thalamus (Figure 1A). This was followed by mouse craniotomy, and two-photon *in-vivo* axonal imaging, while mice are trained in a cued lever-press task (Figure 1 A-D). In this task, a lever press beyond a set threshold during a cue is rewarded with water. Mice are trained with this task daily for two weeks. Training in this task results in more stereotyped lever movements over time, and learning this task was previously shown to be M1 dependent (Chen et al., 2015). M1 dependency was also confirmed by histology slices (Figure 2 A-B). Mice after performing the task for 14 days were perfused and the brain slices were imaged under a confocal microscope. M1 was located according to the coronal mouse brain atlas ("Interactive Atlas Viewer :: Atlas Viewer," n.d.), and fluorescence signals at M1 showed that thalamocortical inputs were ipsilateral, cM1 and S1 inputs were contralateral. An increase in fluorescence signal at L2/3 and deeper layers of M1 shows that inputs were sent out from cM1, S1, and the motor thalamus, and it was integrated at M1 (Figure 2B).

Motor learning is defined as any experience-dependent improvement in performance (Krakauer et al., 2019), and mice performing this lever-press task demonstrated this type of improvement in behavior (Figure 3 A-C). Mice (n=17). On average, they started with gaining 55 rewards in the beginning of training, and reward number increased to around 90 at the end of day 14 (Figure 3A). The number of rewards increased over 60% across 14 sessions. After training, mice also needed less time to react after they heard the cue sound. Across sessions, the average reaction time decreased from around 0.8 sec to 0.2 sec, the reduction in time is about 76% (Figure 3B). The average time mice spent to obtain a reward after the cue sound decreased 60%, from

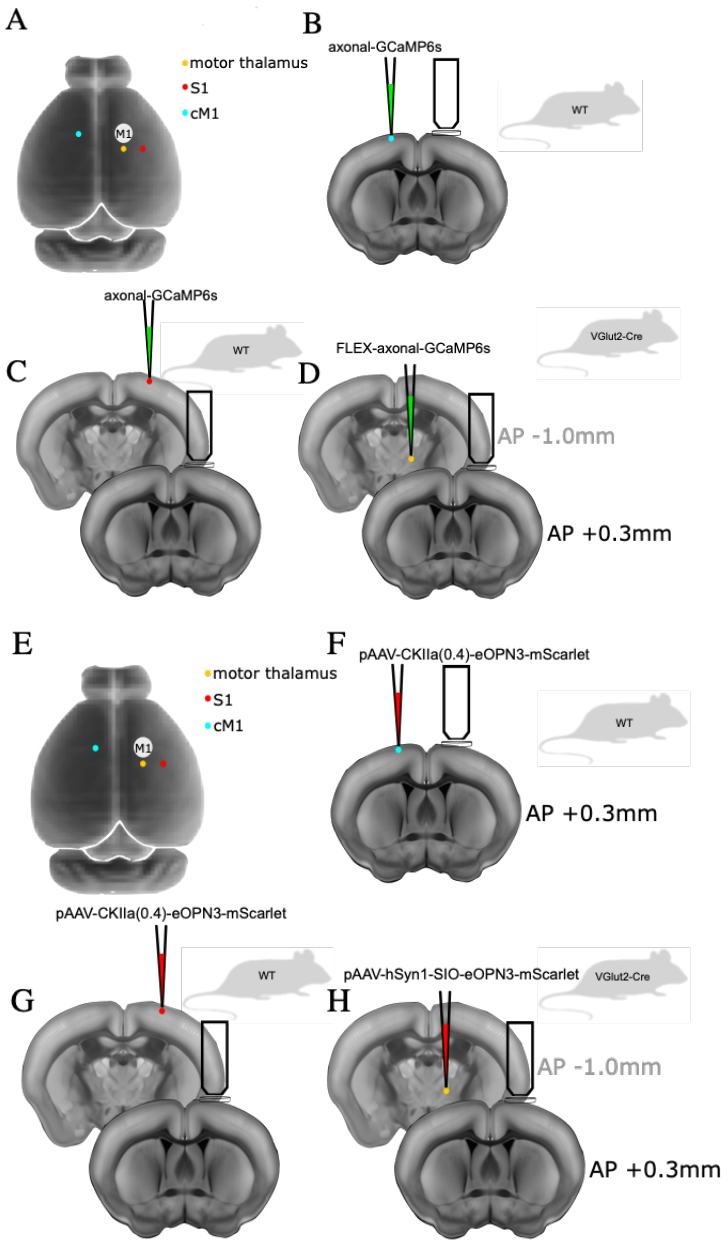

Figure 1. Experimental scheme

(A) Overview of 3 GCaMP6s injection sites: cM1, S1, and motor thalamus.

(B) cM1 injection was performed on the brain of a wild-type mouse (AP 0.3 mm; ML -1.5 mm; DV -0.5/-0.25 mm).

(C) S1 injection was performed on the brain of a wild-type mouse (AP -0.5 mm; ML 2.5 mm; DV -0.5/-0.25 mm).

(D) Thalamocortical injection was performed on the brain of a VGlut2-Cre mouse (AP -1.0 mm; ML 1.0 mm; DV -3.7 mm).

(E) Overview of 3 eOPN3 injection sites: cM1, S1, and motor thalamus.

(F)-(H) Same coordinates as for GCaMP6s injections were used in eOPN3 injections.

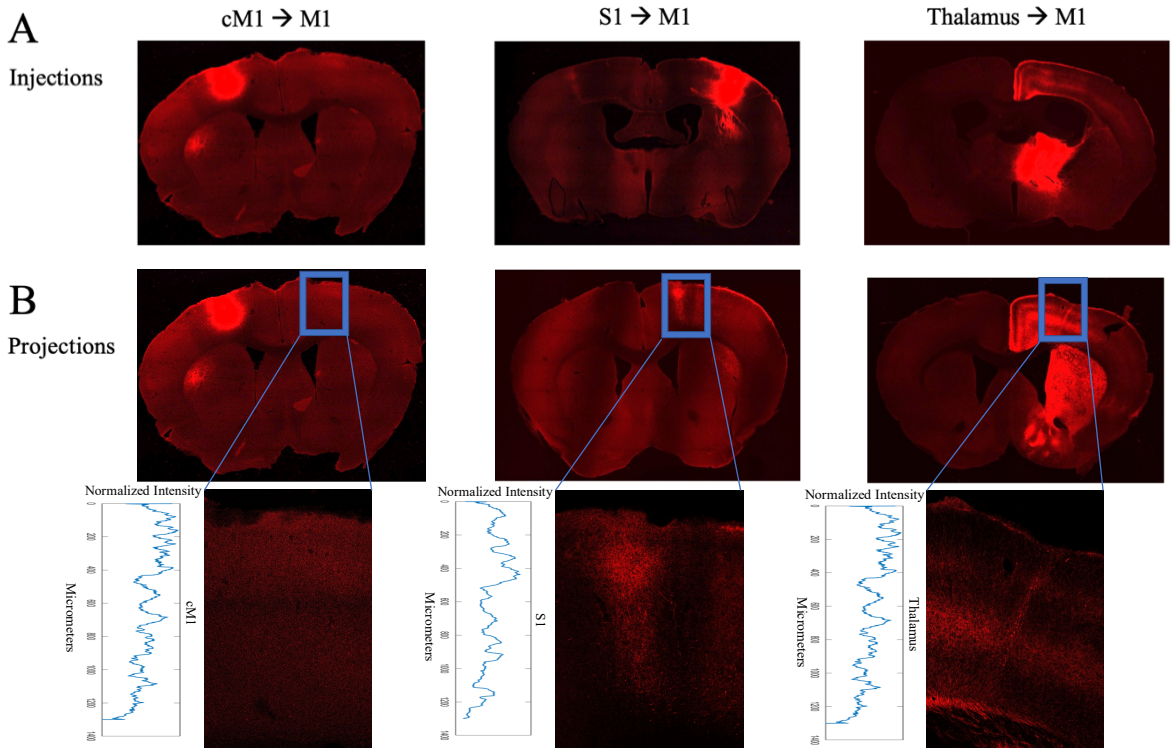

Figure 2. Histology slices of 3 projections in mScarlet

(A) Visualization of virus injection sites for cM1, S1, and the motor thalamus.

(B) Fluorescence signals observed in M1.

around 2 sec to 0.8 sec after 14 days of training (Figure 3C). Across 14 days, the correlation between movement measured in lever traces from different session also increased. Correlation between movement increased from around 0.3 between early sessions (session 1-3), to around 0.36 between late session (session 12-14) (Figure 3D). Comparing movement traces to all the traces within its session, correlation also escalated from around 0.36 to around 0.42 (Figure 3D) showing the movement was becoming more consistent in later sessions.

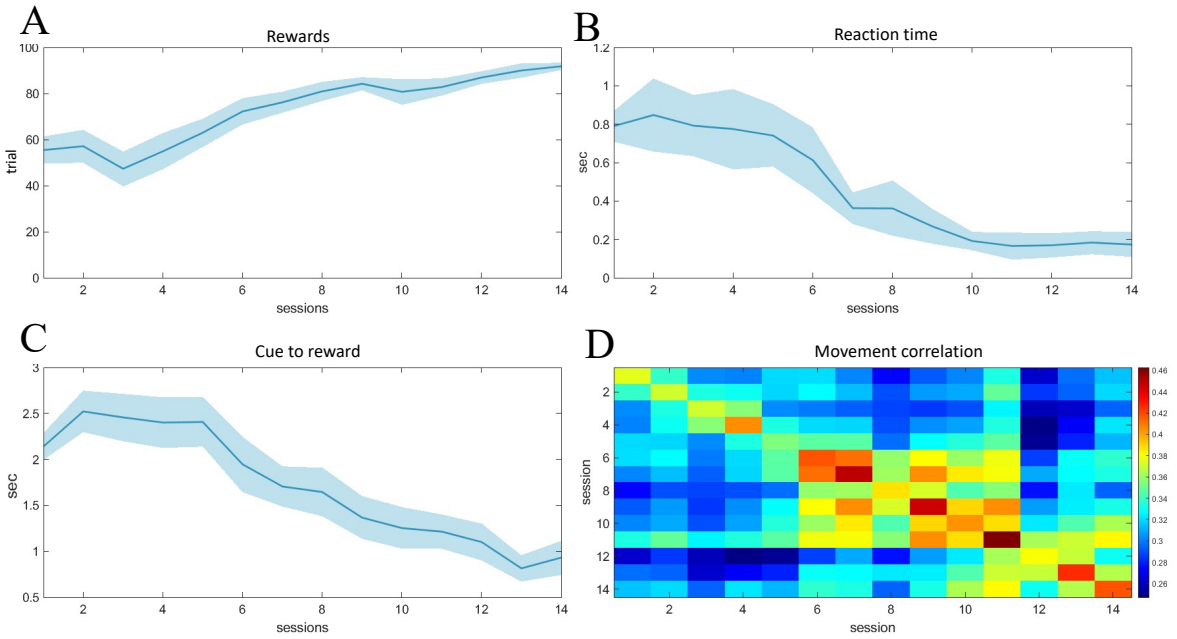

Figure 3. Behavioral changes during the 14-day motor learning

(A) Across 14 sessions, the average reward number with standard error of mean (SEM0 in the lever-press task increased from around 55 to 90.

(B) The average time with SEM of mice used to initiate movement after they heard the tone was shortened from around 0.8 sec to 0.2 sec.

(C) The average time with SEM of mice used to push the lever to pass the thresholds and get water reward after the tone was shortened from around 2 sec to 0.9 sec.

(D) Comparison between sessions revealed an increasing correlation in movement across days. Comparison within sessions revealed an increasing correlation in movement in the same day.

To further analyze the relationship between movement and ROI (region of interest, here it is the axonal bouton) activity, movement traces were smoothened due to the presence of lever movement artifact. Smoothened movement traces were binarized, and each orange block represents a movement initiated by the left limb (Figure 4A). The movement traces were then aligned to ΔF/F and deconvolved spikes (Figure 4B). Since calcium traces used by ΔF/F are delayed at showing the true peak time of axonal boutons, and the slow decay of calcium traces were also not accurate at reflecting the true ROI activity, therefore, deconvolution was used to generate spikes to reflect the true peak times (Pachitariu et al., 2017), where the movement traces were aligned to and showed a correlation between ROI activity and behavior.

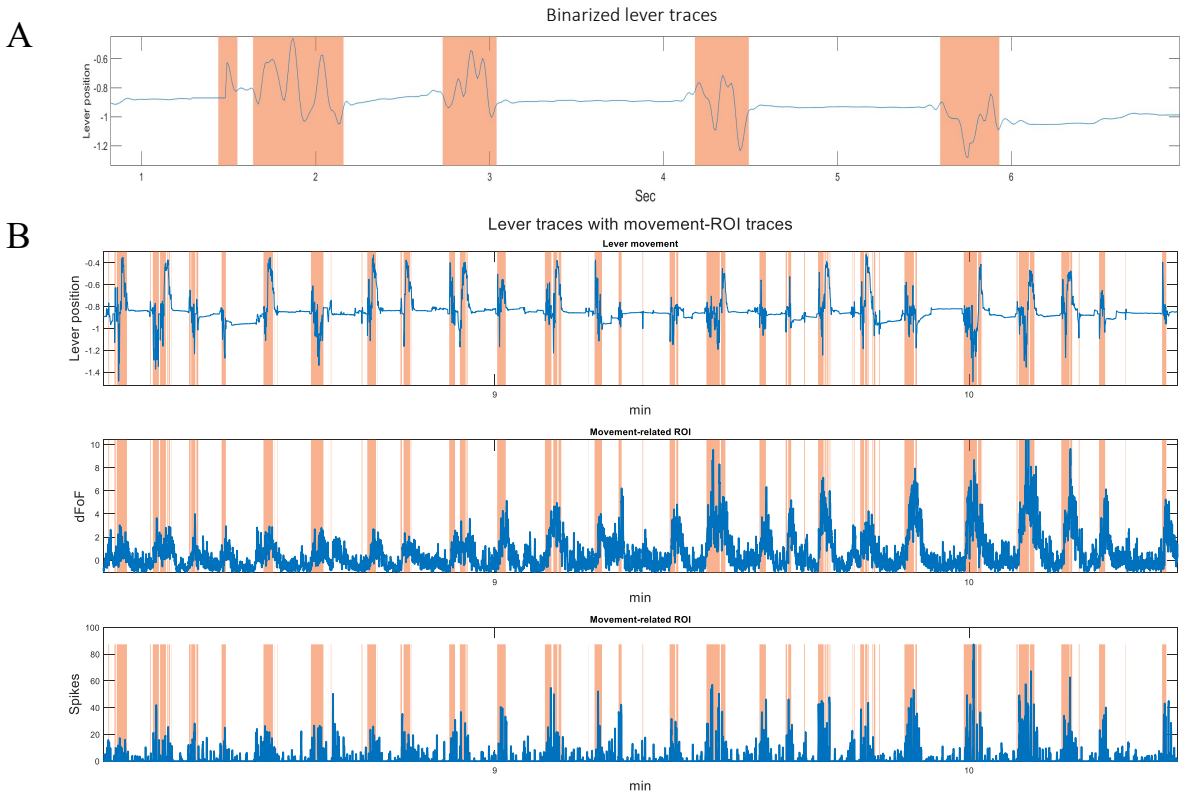

Figure 4. Binarized behavior traces aligned to axonal bouton activity

(A) Lever traces were binarized. Each orange block represents a left limb movement, and it was aligned to lever traces.

(B) Binarized behavior traces were aligned to ΔF/F and deconvolved spikes.

Alignment of movement traces to deconvolved spikes allowed the classification of axonal boutons across projection sites (Figure 5 A-C). For cM1 inputs, on average, movement-related boutons had a higher fraction (~30%) than other types including cue-related (~0.01%), pre-movement-related (~0.1%), and quiescent-related boutons (~0.2%) (Figure 5A). For S1 inputs, movement-related boutons also had a significantly higher fraction (~50%) among all boutons including cue-related (~0.01%), pre-movement-related (~0.1%), and quiescent-related boutons (~0.1%) (Figure 5A). Similar pattern was observed in thalamocortical inputs, movement-related boutons had a higher fraction (~55%), and fractions of others were not as high including cue-related (~0.01%), pre-movement-related (~0.1%), and quiescent-related boutons (~0.2%) (Figure

5A). Although for all projection sites, the fraction of movement—related boutons decreased across sessions, it stayed as the highest among these four classes of boutons. Therefore, inputs from cM1, S1, and the motor thalamus had a higher chance of containing information about movement, and were less likely to carry cue-related, pre-movement-related, and quiescent-related information.

Peak times of movement-related axonal boutons were then aligned along time with a reference to movement onset (shown in black dashed line) (Figure 6A & 6D). Each row represents the average activity traces of an ROI across trials. The bended peak line indicated that the ROI peak time was not randomly distributed across time. A significant fraction of ROI's had their activity maximum immediately followed the movement-onset (0-0.5 sec after) (Figure 6A-D). In both beginner and expert mice, for cM1 and thalamocortical inputs, peak times were right after movement-onset (0-0.5 sec after), but in expert mice, some peaks became late (Figure 6 B-C). For S1 inputs, in beginner mice, similar pattern was observed, but in experts, a significant number of peak times became more randomly distributed 0.5 sec after onset (Figure 6 B-C). Across three types of inputs and the 14-day sessions, peak time became later in expert mice as a change in individual ROI peak time after motor learning (Figure 6 B-C).

In order to examine the relationship between specific projections and learned movement, the average deconvolved spikes of movement-related axonal boutons were aligned to the lever movement onset and offset (Figure 7 A-B). Analyzing only these movement-related boutons showed two clear peaks in activity. The first peak was immediately following movement-onset and the second peak was during movement-end (Figure 7 A-B). The second peak was obvious for thalamocortical inputs, but not so for S1 inputs. To better visualize the changes happened during motor learning, mice in trial 1-3 were grouped as beginners, and mice in trial 12-14 were experts. Thalamocortical boutons showed increased activity during pre-movement and at movement-onset

across all sessions (Figure 7A). These inputs also started increasing its activity before movement-onset started and before any changes happened in other inputs (Figure 7A). In contrast, cM1 axonal boutons became more active during movement in expert mice (Figure 7A). S1 inputs were less active during pre-movement but became more active following movement onset (Figure 7A).

In order to examine different groups of movement-related axonal boutons in terms of peak time, ROIs were sorted into 4 clusters based on temporal sequence from the fastest onset to the slowest (Figure 8 A-B). The first two clusters can be defined as movement-onset related (Figure 8A). The third and fourth clusters represent sustained activity after movement-onset (Figure 8A). In the first two early clusters in reference to movement-onset, peak times of cM1 and thalamocortical inputs were more refined; cM1 peak times were slightly later than thalamocortical inputs (Figure 8A). S1 inputs had the slowest peak onset, and the peak time was more spread out compared to other two projection sites (Figure 8A). In reference to movement-offset, cM1 and thalamocortical inputs exhibited more refined clusters and clear peaks at the behavior end, while for S1 inputs, this type of pattern was not seen (Figure 8B).

A movement-related axonal bouton can have different peak times when comparing to other boutons, and its peak time can also vary across sessions. In order to examine the correlation of individual ROI peak time across sessions, individual ROI activity traces were used to generate a pairwise correlation (Figure 9 A-B). Comparing to themselves across sessions, more movement-related axonal boutons had lower correlation in expert mice (Figure 9 A). In both beginner and expert mice, cM1 input activity was the least correlated to itself, while the thalamocortical ones were the most correlated indicating a more consistent activity pattern across sessions (Figure 9B).

Figure 5. Classification of axonal boutons across projection sites

(A) cM1: average fraction with SEM of movement-related boutons, cue-related boutons, pre-movement-related boutons, and quiescent-related boutons.

(B) S1: average fraction with SEM of movement-related boutons, cue-related boutons, pre-movement-related boutons, and quiescent-related boutons.

(C) Thalamus: average fraction with SEM of movement-related boutons, cue-related boutons, pre-movement-related boutons, and quiescent-related boutons.

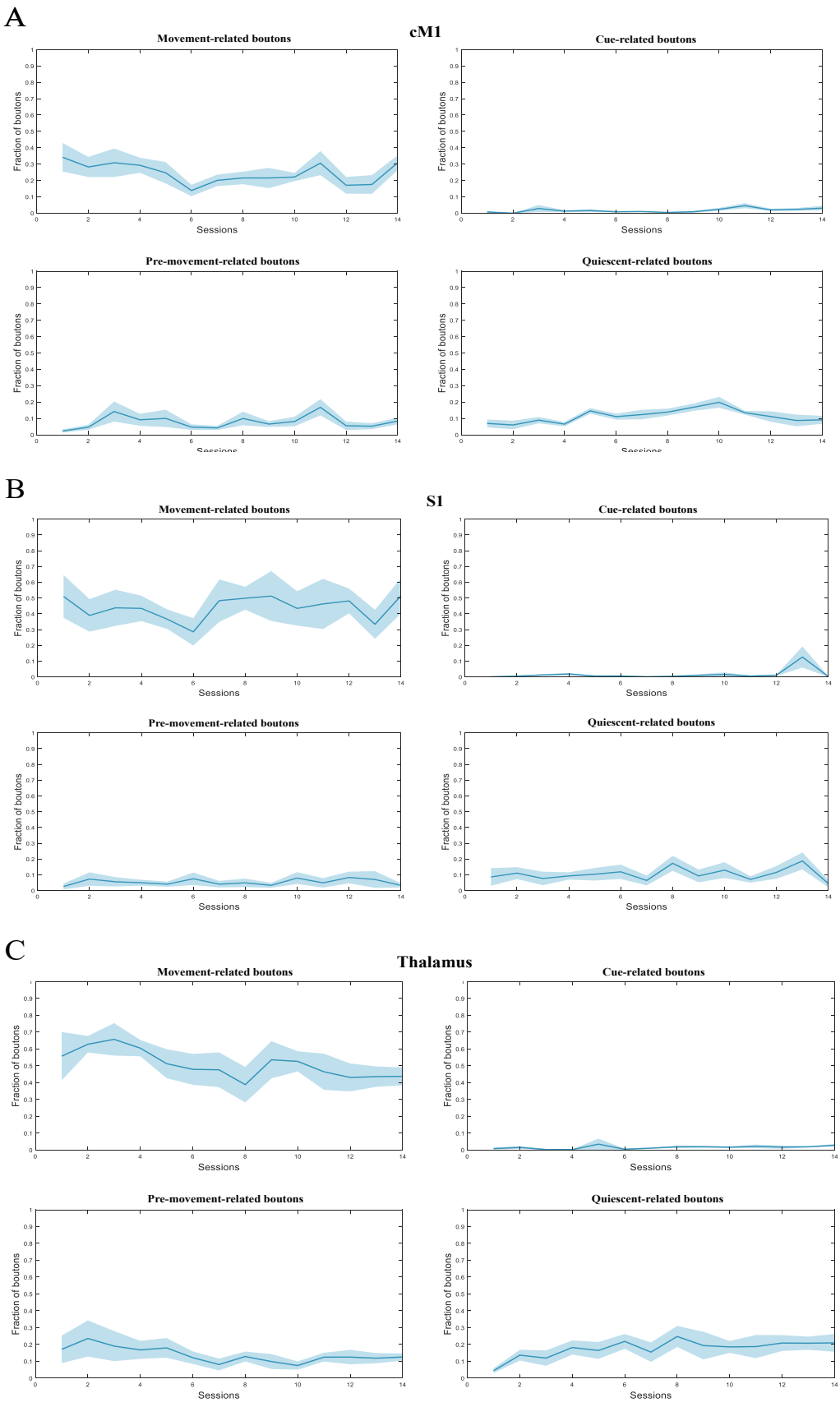
A
cM1
Movement-related boutons
Cue-related boutons
Pre-movement-related boutons
Quiescent-related boutons
B
S1
Movement-related boutons
Cue-related boutons
Pre-movement-related boutons
Quiescent-related boutons
C
Thalamus
Movement-related boutons
Cue-related boutons
Pre-movement-related boutons
Quiescent-related boutons
Fraction of boutons
Sessions

Since axonal bouton activity was correlated with movement, in order to decipher the functional role of M1 inputs, neurotransmitter release at synaptic terminals were suppressed with eOPN3. AAV-eOPN3-mScarlet was injected into cM1, S1, and motor thalamus (Figure 1E-H). 1 month was waited for virus to express and the same behavior paradigm as for GCaMP6s imaging was used (Figure 1F-H).

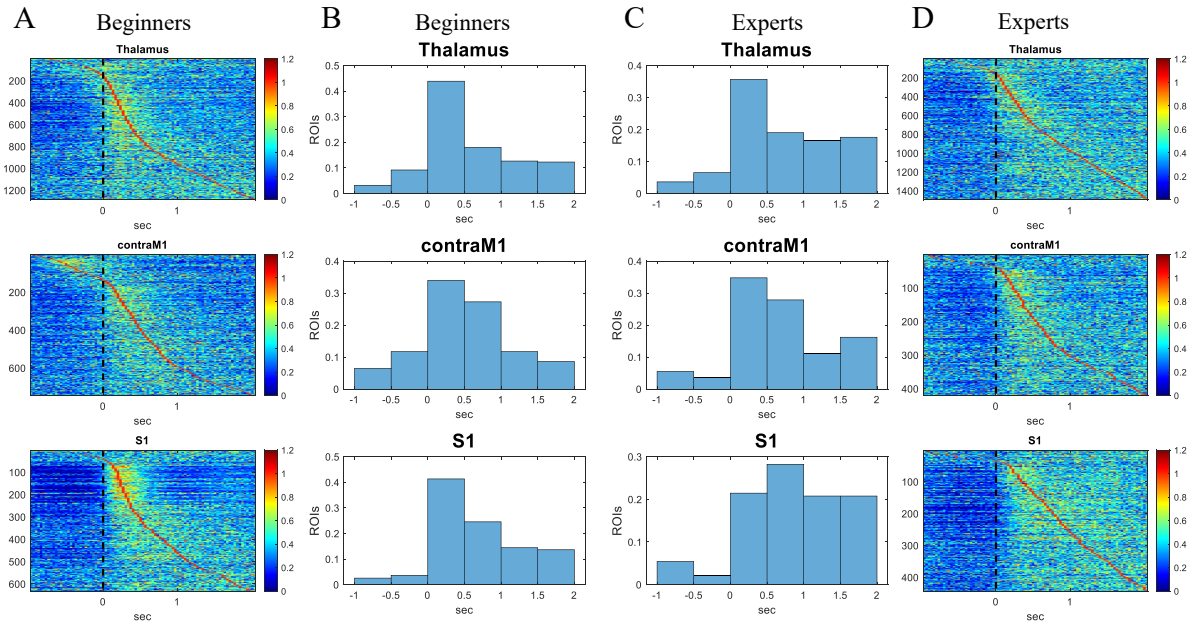

Figure 6. Individual deconvolved spikes of movement-related axonal boutons aligned to movement onset

(A) Individual deconvolved spikes of movement related axonal boutons in beginner mice were aligned to movement onset.

(B) Normalized histogram shows the fractions of movement related axonal boutons in beginner mice at different peak times.

(C) Normalized histogram shows the fractions of movement related axonal boutons in expert mice at different peak times.

(D) Individual deconvolved spikes of movement related axonal boutons in expert mice were aligned to movement onset.

A

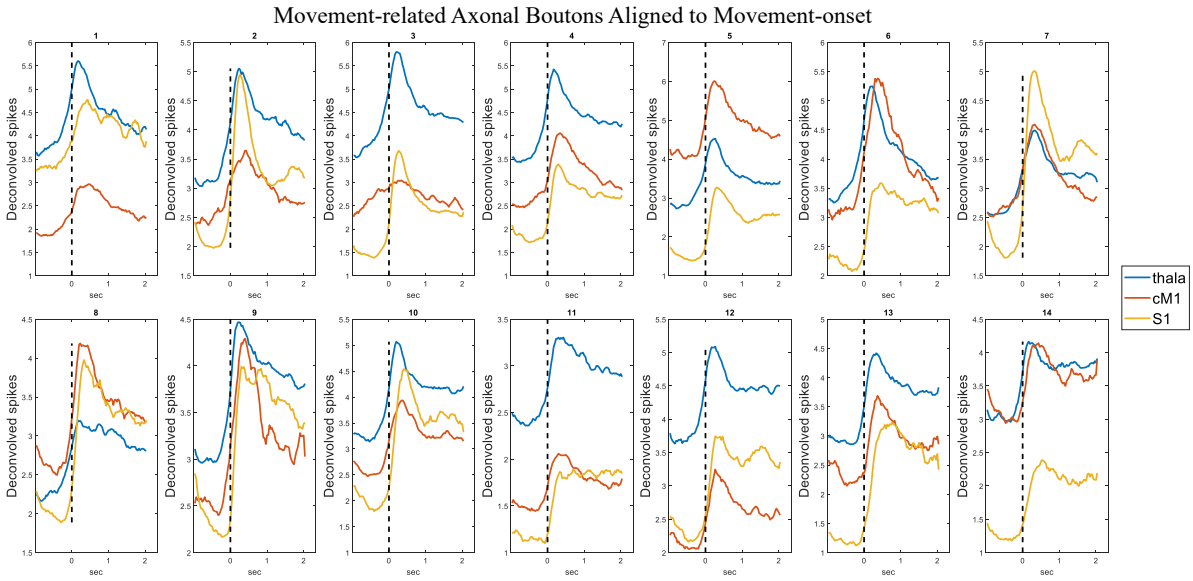

B

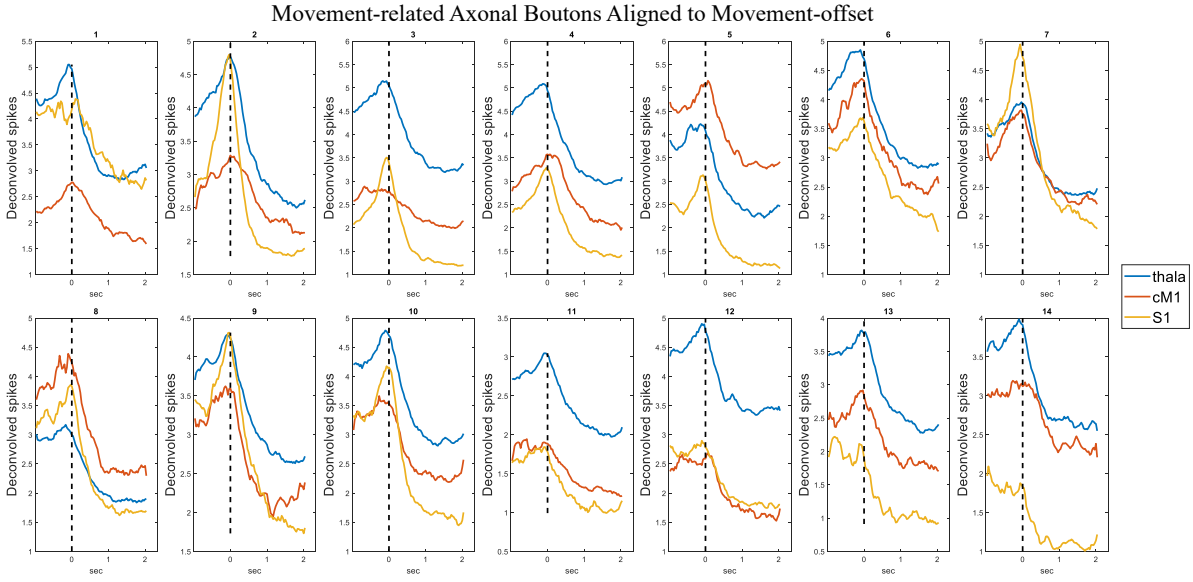

Figure 7. Averaged deconvolved spikes of movement-related axonal boutons aligned to movement onset and offset

(A) Activity traces of movement related axonal boutons were aligned to the movement-onset.

(B) Activity traces of movement related axonal boutons were aligned to the movement-offset.

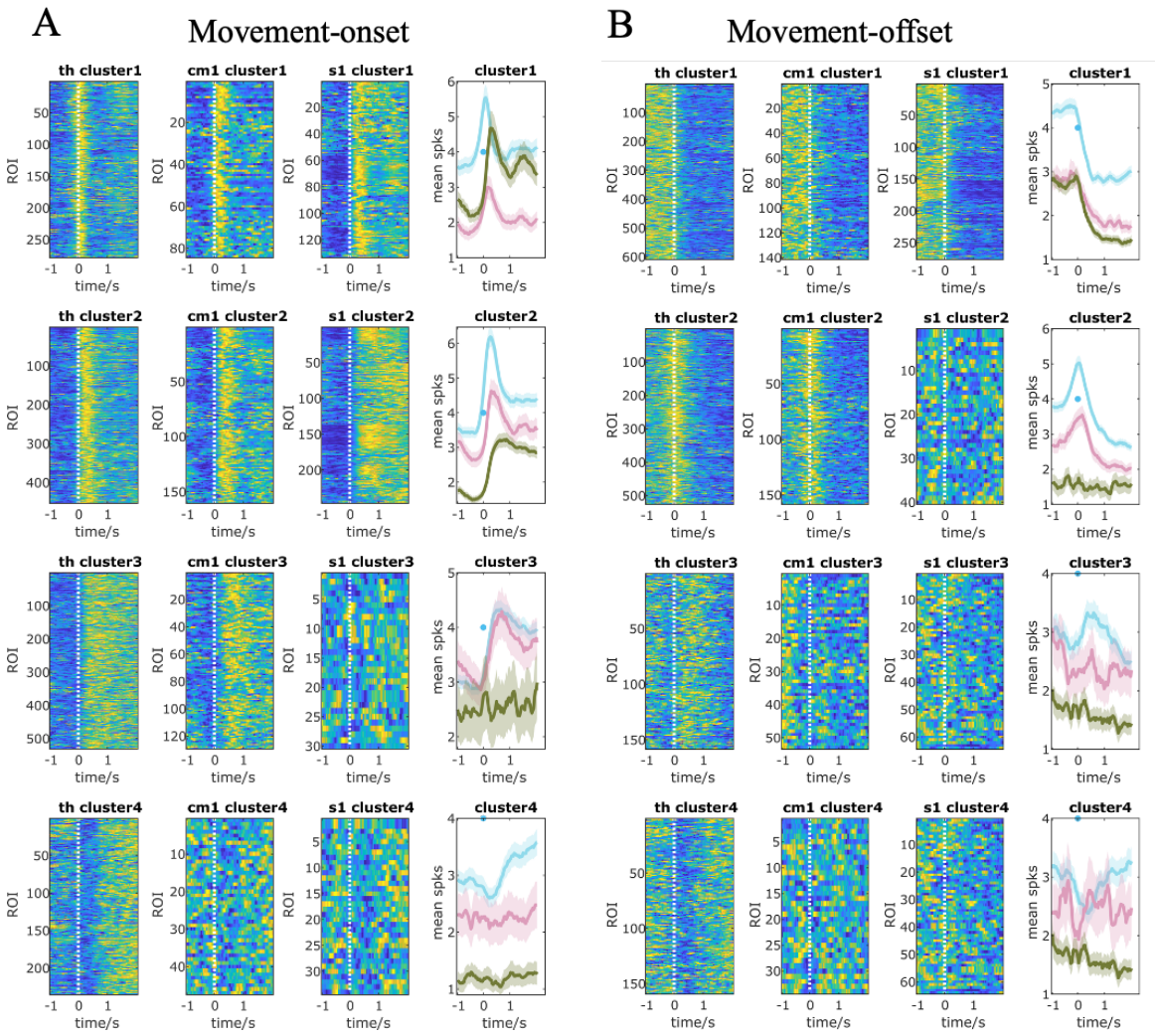

Figure 8. Movement-related boutons grouped into 4 clusters based on peak time in the temporal sequence

(A) Blue line represents thalamocortical inputs; pink line represents cM1 inputs; green line represents S1 inputs. Movement-related boutons from three projection sites were sorted into 4 clusters in reference to the movement-onset.

(B) Movement-related boutons from three projection sites were sorted into 4 clusters in reference to the movement-offset.

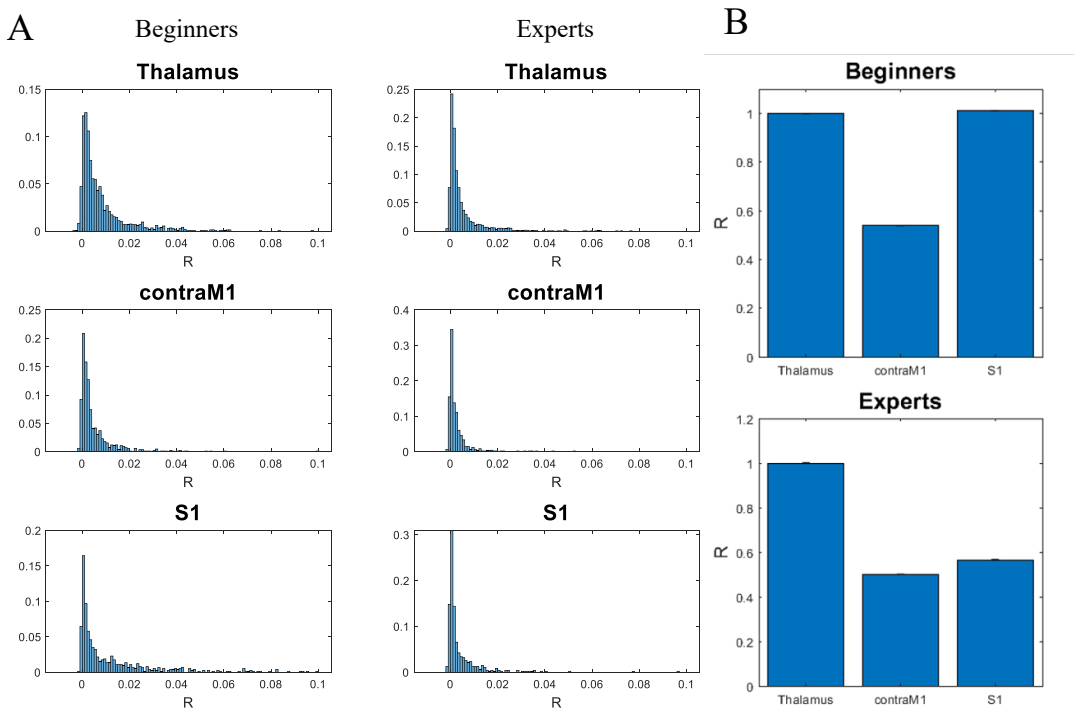

Figure 9. Pairwise comparison of individual axonal bouton activity across trials

(A) Activity of individual axonal bouton was compared to itself in the first 3 sessions.

(B) Activity of individual axonal bouton was compared to itself in the last 3 sessions.

(C) Comparison of the correlation of individual ROI activity in three M1 inputs across days.

Discussion:

Training mice in the cued lever-press task resulted in an increased success rate and fastest reaction time. During motor learning, lever presses became more stereotype, and correlated both between sessions and within each session. r. Binarized movement traces were aligned to M1 axonal bouton's activity peaks, and the movement traces were shown be correlated with ROI activity. The alignment of individual ROI peak time to movement-onset and offset also reflected the correlation between ROI activity and movement-onset and offset. Further analysis showed that in all boutons, the fraction of movement-related boutons was significantly higher than other classes (cue-related, pre-mov related, and quiescent boutons), but this number tended to decrease slightly across sessions. This is consistent with the finding that M1 is critical for certain motor skills especially goal-directed movement (Chen et al., 2015).

Since the motor cortex does not function in isolation, rather it is part of a relay system, where it receives major inputs from cM1, S1, and the motor thalamus, and it integrates the information and sends out different inputs (Hooks et al., 2013; Penhune and Steele, 2012). To answer the question whether these inputs are the same during motor learning, meaning they are redundant, or they are completely different and have various function, activity of major M1 inputs was analyzed. When population average of ROI activity was aligned to movement-onset and offset, two peaks were observed immediately after movement-onset and right at movement-offset, and also in expert mice, ROI activity peaked later in time following movement-onset. Differences were also present, thalamocortical inputs were consistently the most active before movement starts, during movement, and at movement end. cM1 inputs became more active after movement-onset. S1 inputs were the least active during pre-movement period but became more active following movement onset. In terms of movement-offset, thalamocortical inputs exhibited a more obvious

peak at movement-end, but there was no obvious peak for S1 inputs. Therefore, the population average of activity of the three major M1 inputs was quite different during motor learning.

Based on the difference in peak time, movement-related ROIs were sorted into clusters. Axonal boutons from different projection site exhibited different peak patterns in terms of clusters. Thalamocortical inputs had the fastest onset and the most refined peak times in both beginner mice and expert mice, while S1 had the slowest onset, and its peak times were very spread out. The consistency in thalamocortical ROI activity was also observed when comparing individual ROI activity across trails. The same thalamocortical ROI was more likely to peak at the same time. However, cM1 input activity would be the most random compared to the other two types of inputs. Thus, these three M1 major inputs had distinct activity patterns during motor learning. One of the possible reasons for this pattern in clustering is probably because of the different roles of each brain regions. S1 is responsible for providing sensory feedback, and therefore inputs from S1 might be variable and therefore the activity pattern is more random (Petrof et al., 2015). Since sensory feedback is not as important in the temporal sequence during motor learning, its peak time is not as refined as inputs from the motor thalamus, which has critical roles in movement initiation and termination for learned motor skills (Sauerbrei et al., 2020; Tanaka et al., 2018). Since cM1 inputs have the role in assisting bilateral movements and suppressing unilateral movements, and they can also innervate neurons in all layers of M1, the activity pattern of cM1 can be more variable and makes it harder to define (Muñoz-Castañeda et al., 2020).

References

1. Broussard, G.J., Liang, Y., Fridman, M., Unger, E.K., Meng, G., Xiao, X., Ji, N., Petreanu, L., Tian, L., 2018. In vivo measurement of afferent activity with axon-specific calcium imaging. Nat. Neurosci. 21, 1272–1280. https://doi.org/10.1038/s41593-018-0211-4

2. Chen, S.X., Kim, A.N., Peters, A.J., Komiyama, T., 2015. Subtype-specific plasticity of inhibitory circuits in motor cortex during motor learning. Nat. Neurosci. 18, 1109–1115. https://doi.org/10.1038/nn.4049

3. Hira, R., Ohkubo, F., Tanaka, Y.R., Masamizu, Y., Augustine, G.J., Kasai, H., Matsuzaki, M., 2013. In vivo optogenetic tracing of functional corticocortical connections between motor forelimb areas. Front. Neural Circuits 7. https://doi.org/10.3389/fncir.2013.00055

4. Holtmaat, A., Bonhoeffer, T., Chow, D.K., Chuckowree, J., De Paola, V., Hofer, S.B., Hübener, M., Keck, T., Knott, G., Lee, W.-C.A., Mostany, R., Mrsic-Flogel, T.D., Nedivi, E., Portera-Cailliau, C., Svoboda, K., Trachtenberg, J.T., Wilbrecht, L., 2009. Long-term, high-resolution imaging in the mouse neocortex through a chronic cranial window. Nat. Protoc. 4, 1128–1144. https://doi.org/10.1038/nprot.2009.89

5. Hooks, B.M., Mao, T., Gutnisky, D.A., Yamawaki, N., Svoboda, K., Shepherd, G.M.G., 2013. Organization of Cortical and Thalamic Input to Pyramidal Neurons in Mouse Motor Cortex. J. Neurosci. 33, 748–760. https://doi.org/10.1523/JNEUROSCI.4338-12.2013

6. Hwang, E.J., Dahlen, J.E., Hu, Y.Y., Aguilar, K., Yu, B., Mukundan, M., Mitani, A., Komiyama, T., 2019. Disengagement of motor cortex from movement control during long-term learning. Sci. Adv. 5, eaay0001. https://doi.org/10.1126/sciadv.aay0001

7. Interactive Atlas Viewer :: Atlas Viewer [WWW Document], n.d. URL http://atlas.brain-map.org/atlas?atlas=1#atlas=1&plate=100960224&structure=549&x=5280.132533482143&y=3744.0129743303573&zoom=-3&resolution=11.97&z=5 (accessed 5.11.21).

8. Kawai, R., Markman, T., Poddar, R., Ko, R., Fantana, A.L., Dhawale, A.K., Kampff, A.R., Ölveczky, B.P., 2015. Motor Cortex Is Required for Learning but Not for Executing a Motor Skill. Neuron 86, 800–812. https://doi.org/10.1016/j.neuron.2015.03.024

9. Komiyama, T., Sato, T.R., O'Connor, D.H., Zhang, Y.-X., Huber, D., Hooks, B.M., Gabitto, M., Svoboda, K., 2010. Learning-related fine-scale specificity imaged in motor cortex circuits of behaving mice. Nature 464, 1182–1186. https://doi.org/10.1038/nature08897

10. Krakauer, J.W., Hadjiosif, A.M., Xu, J., Wong, A.L., Haith, A.M., 2019. Motor Learning, in: Comprehensive Physiology. American Cancer Society, pp. 613–663. https://doi.org/10.1002/cphy.c170043

11. Mahn, M., Saraf-Sinik, I., Patil, P., Pulin, M., Bitton, E., Karalis, N., Bruentgens, F., Palgi, S., Gat, A., Dine, J., Wietek, J., Davidi, I., Levy, R., Litvin, A., Zhou, F., Sauter, K., Soba, P., Schmitz, D., Lüthi, A., Rost, B.R., Wiegert, J.S., Yizhar, O., 2021. Optogenetic silencing of neurotransmitter release with a naturally occurring invertebrate rhodopsin. bioRxiv 2021.02.18.431673. https://doi.org/10.1101/2021.02.18.431673

12. Makino, H., Ren, C., Liu, H., Kim, A.N., Kondapaneni, N., Liu, X., Kuzum, D., Komiyama, T., 2017. Transformation of Cortex-wide Emergent Properties during Motor Learning. Neuron 94, 880-890.e8. https://doi.org/10.1016/j.neuron.2017.04.015

13. Muñoz-Castañeda, R., Zingg, B., Matho, K.S., Wang, Q., Chen, X., Foster, N.N., Narasimhan, A., Li, A., Hirokawa, K.E., Huo, B., Bannerjee, S., Korobkova, L., Park, C.S., Park, Y.-G., Bienkowski, M.S., Chon, U., Wheeler, D.W., Li, Xiangning, Wang, Yun, Kelly, K., An, X., Attili, S.M., Bowman, I., Bludova, A., Cetin, A., Ding, L., Drewes, R., D'Orazi, F., Elowsky, C., Fischer, S., Galbavy, W., Gao, L., Gillis, J., Groblewski, P.A., Gou, L., Hahn, J.D., Hatfield, J.T., Hintiryan, H., Huang, J., Kondo, H., Kuang, X., Lesnar, P., Li, Xu, Li, Y., Lin, M., Liu, L., Lo, D., Mizrachi, J., Mok, S., Naeemi, M., Nicovich, P.R., Palaniswamy, R., Palmer, J., Qi, X., Shen, E., Sun, Y.-C., Tao, H., Wakemen, W., Wang, Yimin, Xie, P., Yao, S., Yuan, J., Zhu, M., Ng, L., Zhang, L.I., Lim, B.K., Hawrylycz, M., Gong, H., Gee, J.C., Kim, Y., Peng, H., Chuang, K., Yang, X.W., Luo, Q., Mitra, P.P., Zador, A.M., Zeng, H., Ascoli, G.A., Huang, Z.J., Osten, P., Harris, J.A., Dong, H.-W., 2020. Cellular Anatomy of the Mouse Primary Motor Cortex. bioRxiv 2020.10.02.323154. https://doi.org/10.1101/2020.10.02.323154

14. Pachitariu, M., Stringer, C., Dipoppa, M., Schröder, S., Rossi, L.F., Dalgleish, H., Carandini, M., Harris, K.D., 2017. Suite2p: beyond 10,000 neurons with standard two-photon microscopy. bioRxiv 061507. https://doi.org/10.1101/061507

15. Penhune, V.B., Steele, C.J., 2012. Parallel contributions of cerebellar, striatal and M1 mechanisms to motor sequence learning. Behav. Brain Res. 226, 579–591. https://doi.org/10.1016/j.bbr.2011.09.044

16. Peters, A.J., Chen, S.X., Komiyama, T., 2014. Emergence of reproducible spatiotemporal activity during motor learning. Nature 510, 263–267. https://doi.org/10.1038/nature13235

17. Petrof, I., Viaene, A.N., Sherman, S.M., 2015. Properties of the primary somatosensory cortex projection to the primary motor cortex in the mouse. J. Neurophysiol. 113, 2400–2407. https://doi.org/10.1152/jn.00949.2014

18. Sauerbrei, B.A., Guo, J.-Z., Cohen, J.D., Mischiati, M., Guo, W., Kabra, M., Verma, N., Mensh, B., Branson, K., Hantman, A.W., 2020. Cortical pattern generation during dexterous movement is input-driven. Nature 577, 386–391. https://doi.org/10.1038/s41586-019-1869-9

19. Tanaka, K.Z., He, H., Tomar, A., Niisato, K., Huang, A.J.Y., McHugh, T.J., 2018. The hippocampal engram maps experience but not place. Science 361, 392–397. https://doi.org/10.1126/science.aat5397